

Adhesion of elastic microbeams on thin deformable substrates

Hang Li, Zhaohe Dai ^{*}

Department of Mechanics and Engineering Science, State Key Laboratory for Turbulence and Complex Systems, College of Engineering, Peking University, Beijing 100871, China

ARTICLE INFO

Keywords:
Adhesion
Stiction
Thin elastic layer
Delamination
Van der Waals forces

ABSTRACT

We revisit the adhesion problem of microbeams by considering thin elastic substrates and long-range interfacial forces, inspired by recent experiments in flexible electronics and micro/nano electromechanical systems (M/NEMS). Previously, this problem has been extensively analyzed for rigid substrates using a Johnson–Kendall–Roberts (JKR) or Griffith-type adhesion criterion, which involves applying a discontinuity condition across the adhesion front as a critical boundary condition. Our study demonstrates that this critical adhesion condition can be *qualitatively* altered when the substrate deformation is taken into account. We introduce a single parameter to determine when the effect of substrate elasticity should be considered or can be neglected. For structures at small scales, we replace the JKR-type jump conditions with a smoothed interfacial law, specifically the Lennard-Jones potential in this work. We then discuss the small-scale adhesion behavior of microbeams with thin deformable substrates and examine how this behavior transitions back to Griffith-type adhesion as the system's length scale increases. These findings have direct implications for the design and reliability of M/NEMS and microfluidic devices, especially those developed or encapsulated with deformable substrates.

1. Introduction

The unintentional adhesion of mechanical and functional structures to substrates is a common cause of malfunction in micro/nano-electro-mechanical systems (M/NEMS) [1,2]. This phenomenon, often termed stiction, frequently occurs in small-scale slender structures such as microbeams, cantilevers, ultra-thin plates, and 2D crystals [3–5]. The underlying mechanism of stiction is simply that the area-related adhesive forces become considerable enough compared to the volume-related elastic forces as the smallest dimension of a structure (usually thickness) is below the millimeter level [3,4]. Although stiction has raised serious reliability concerns in traditional MEMS [3], recent advances in MEMS, stretchable electronics [6], and microfluidics [7] have taken advantage of the stiction configuration to achieve specific functions, such as nano-switches [8], tough-down pressure sensors [9,10], and 3D buckled micro-architectures [11,12]. To either mitigate or exploit stiction in various applications, it is crucial to develop a theoretical framework capable of predicting the stiction behavior of small-scale slender structures [3,13].

Extensive research has focused on the stiction problem involving rigid substrates [14–16], particularly examining the criteria for stiction occurrence and the geometry of a stictioned structure on a substrate [17–21]. A common model involves an elastic cantilever positioned above a rigid substrate with a small gap. For instance, Mastrangelo and Hsu analyzed the mechanical stability of such geometries under both capillary and adhesive forces acting at the structure–substrate gap, employing a JKR-type approach, which minimizes the total free energy by considering surface and interface energies [17,18]. Furthermore, Mastrangelo discussed the adhering or detaching length of beams and plates with varying geometries in MEMS using this approach [19]. De Boer and

* Corresponding author.

E-mail address: daizh@pku.edu.cn (Z. Dai).

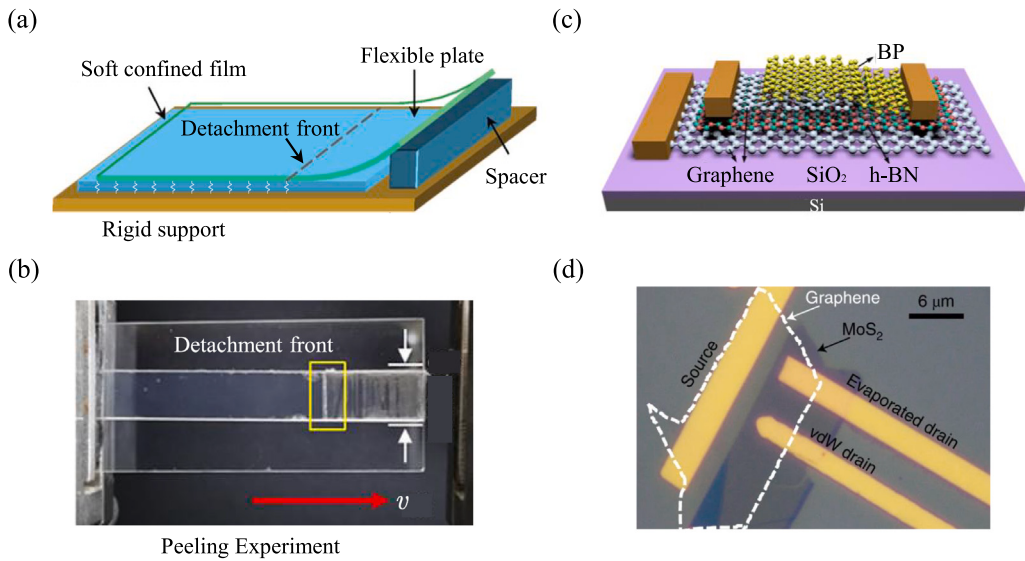


Fig. 1. Adhesion of elastic microbeams/plates on thin, deformable substrates. (a) Schematic of a plate delaminating from a thin elastic film that is bonded to a rigid substrate [32]. Given the slender geometry of the elastic film, it can be considered a Winkler foundation according to [33]. (b) Photograph of relevant experiments in which an elastic plate is peeled from an elastic foundation. [34]; (c) Schematic of a typical 2D material-based electronic device (a field-effect Schottky barrier transistor in this figure) where the functional 2D material plate is placed on top of other layered structures which can also be considered as a transversely isotropic foundation [35]. Such a combined structure is often termed as heterostructure. (d) Optical image of a typical device with graphene/ MoS_2 reported in Ref. [36].

Michalske investigated the microbeam stiction problem using a Griffith-type approach, which evaluates the energy release rate of the system — essentially identical to the JKR-type approach — and applied their analytical results to measure the adhesion of the cantilever beam [20]. Similarly, Rogers et al. [22] calculated the energy release rate while accounting for the temperature effect caused by heating during the sample preparation process. Jones et al. [21] characterized the adhesion of MEMS cantilevers subjected to cyclic point loading, exploring the transitions between freestanding, arc-shaped, and S-shaped equilibrium configurations. Fang et al. [23] considered both the bending energy and the nonlinear stretching energy induced by the transverse deflection of the beam, discussing the impact of geometric nonlinearity on stiction. More recently, the regime diagram of the axisymmetric stiction problem, arising from the interplay of bending, stretching, and pretension effects, has been discussed [24].

Apart from the JKR-type or Griffith-type approaches mentioned above, Glassmaker and Hui calculated the energy release rate in the stiction system by changing the strain energy with an incremental advance in the crack length (the J integral) [25]. This perspective is situated directly at the adhesion or delamination front, resulting in a critical adhesive boundary condition characterized by a jump in the beam's curvature or bending moment [25]. Later, Majidi and coworkers performed a variational analysis and obtained the same adhesive boundary condition, along with the governing equations for the stiction problem of beams and elastica [26,27]. More recently, Kardomateas and colleagues have extended the J integral analysis of the energy release rate for cantilever beam sandwich testing configurations under large deflections [28,29]. The JKR-type, Griffith-type, and J integral approaches are fundamentally identical and can be considered “macroscopic” methods, as they all assume that the presence of an interface can be solely characterized by adhesion energy. Alternatively, when the gap between the beam and substrate reaches sub-micron scales, a Dugdale-type approach, specifically using a Lennard-Jones potential at the interface, appears more appropriate, which has been discussed and validated with experimental results on graphite flakes by Liu et al. [30]. Wagner and Vella [31] further demonstrated numerically that the stiction behavior calculated using the Lennard-Jones potential can consistently recover to the behavior predicted by using the macroscopic jump boundary condition as the characteristic length scale of the system increases.

Although the stiction, adhesion, and delamination of slender structures on rigid substrates have been extensively studied from various perspectives, the development of flexible electronics, microfluidic devices, and M/NEMS has increasingly utilized substrates with certain degrees of deformability. As illustrated in Figs. 1a and 1b, a number of engineering systems have adopted a soft adhesive or elastic coating on the rigid substrate [32,34,37]. At even small-scale systems such as van der Waals material based devices (Figs. 1c and 1d), the functional plate is often placed on a layered (though anisotropic) foundation that is deformable [5,35,38–40]. The introduction of deformable substrates has provided new opportunities in the design and performance of these systems and, at the same time, raised a fundamental question regarding how substrate elasticity influences the stiction or adhesion behavior of these structures. This issue has been discussed in the context of the substrate being an elastic or viscoelastic half-space [41–44]. However, the geometry of the deformable substrates illustrated in Fig. 1 is notably slender. While recent studies have addressed similar problems, such as the peeling of a plate from a thin, incompressible substrate [32,45], it remains unclear how the presence of a thin, compressible substrate would affect the curvature jump condition previously derived for rigid substrates [46]. Additionally,

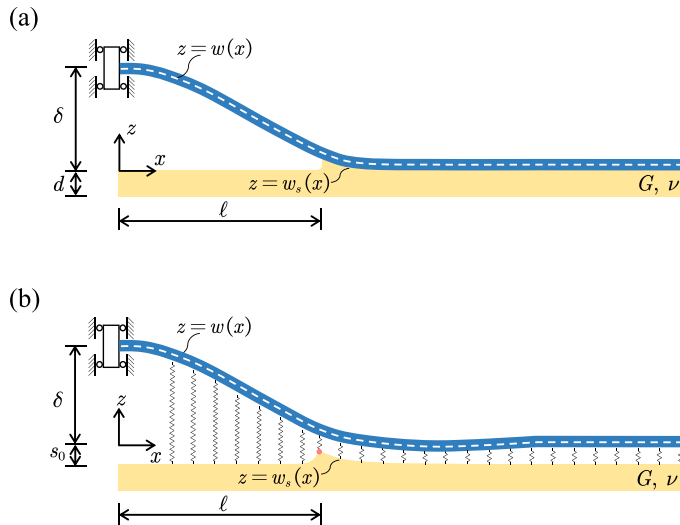


Fig. 2. Schematic illustration and notation for the analysis. (a) The beam or plate, of bending stiffness B , adheres to a thin elastic layer characterized by shear modulus G , Poisson ratio ν , and thickness d . The left end of the plate is lifted with zero slope with a displacement δ and the interface is then delaminated with a delamination length ℓ . The deformations of the neutral axis of the beam and the top surface of the elastic layer are described by $z = w(x)$ and $z = w_s(x)$, respectively. (b) Schematic illustration for the Dugdale-type model in which the beam-substrate interfaced is characterized by a smoothed interfacial law.

at small scales, such as those found in semiconductor devices, there exists a combined effect of long-range interfacial forces and thin elastic substrates that, to the best of our knowledge, has yet to be fully investigated.

In this study, we focus on the adhesion problem of microbeams by examining the effects of thin elastic substrates and long-range interfacial forces. We pay particular attention to how these effects modify the adhesion conditions and behavior of the microbeam, as well as the circumstances under which they can be neglected. The paper is organized as follows: In Section 2, we introduce a Griffith-type model and a Dugdale-type model for addressing this adhesion problem. In Section 3, we discuss the results obtained using the JKR-type model. We show the existence of a characteristic bendoadhesive length in the delaminated region and show that considering thin elastic substrates can introduce a new length scale in the contact region. We then introduce a transition parameter, defined by comparing the length scales in the delaminated and contact regions, and show that this parameter can be used to connect the results for elastic and rigid substrates. Section 4 focuses on the Dugdale-type model and the associated transition parameters. Finally, we conclude with a summary of our main findings in Section 5.

2. Simple models

2.1. Griffith-type approach

We begin by examining a beam of bending stiffness B adhered to a thin elastic layer from a Griffith-type perspective, as illustrated in Fig. 2a. When a prescribed deflection, δ , is applied at the left end ($x = 0$), we denote the beam deflection by $w(x)$ and the substrate surface deformation by $w_s(x)$. Assuming perfect adhesion in the contact region, we have $w = w_s$ for $x > \ell$, where ℓ represents the position of the adhesion or delamination front. Applying linear beam theory, the governing equation of the problem can be expressed as follows:

$$B \frac{d^4 w}{dx^4} + p = 0, \quad (1)$$

for $x \geq 0$, where p is the distributed force acting on the beam, satisfying

$$p = k_w w \mathcal{H}(x - \ell). \quad (2)$$

In the Griffith-type perspective, the distributed force exists only in the contact region ($x > \ell$) and is linearly proportional to the substrate's deformation with a constant stiffness k_w . Therefore, the Heaviside step function \mathcal{H} is used in Eq. (2).

We note that the constant k_w is a physical parameter. For substrates of shear modulus G , thickness d , and Poisson's ratio ν , Skotheim and Mahadevan have used an analogue of hydrodynamic lubrication theory to derive that [33]

$$k_w = \frac{2(1-\nu)}{1-2\nu} \frac{G}{d}. \quad (3)$$

This indicates that a thin substrate can be modeled as a Winkler foundation, which is composed of an array of independent springs with a constant elastic stiffness k_w . Note that this model can reduce to the rigid substrate case as G/d goes infinite but cannot recover the elastic half-space [47,48]. The Winkler foundation model is suitable for describing the deformation of a compressible

thin elastic layer. However, it becomes invalid for complete or nearly incompressible elastomers with strong shear interactions, such as commonly used rubber or polydimethylsiloxane (PDMS). In these materials, the deformation of the foundation is related to the Laplacian of the restoring force, leading to a sixth-order governing differential equation rather than the conventional uncoupled fourth-order equation used in Winkler foundation models [49,50]. It also should be noted that the Winkler foundation requires a large slenderness of the substrate, i.e., the thickness of the substrate must be much smaller than the characteristic horizontal length of the Winkler foundation. In addition, since the Winkler stiffness in Eq. (3) is obtained based on linear elasticity theory, we require the deflection of the substrate to be much smaller than its thickness in the contact domain. Note that recently Chandler and Vella [51] showed that this foundation model remains accurate as long as the Poisson's ratio is not too close to 0.5, i.e., $1-2\nu \gg d/\ell_*$, where ℓ_* is a horizontal length scale in the contacted region (to be discussed in the next section). Moreover, even when the substrate is transversely isotropic (as shown in Fig. 1c), it can still be treated as a Winkler foundation. In this case, the elastic stiffness is given by

$$k_W = C_{33}/d, \quad (4)$$

where C_{33} is an elastic constant for transversely isotropic materials, according to [52,53].

We can readily have a few natural boundary for the problem depicted in Fig. 2a, including

$$w(0) = \delta, \quad w'(0) = 0, \quad w(\infty) = 0, \quad w'(\infty) = 0, \quad (5)$$

where w' denote dw/dx . Unlike the case of a rigid substrate, where there is a jump in the beam curvature across the delamination front [25–27], the presence of a deformable substrate mitigates this discontinuity. Specifically, continuity is maintained up to the level of the shear force in the beam across $x = \ell$:

$$\llbracket w(\ell) \rrbracket = \llbracket w'(\ell) \rrbracket = \llbracket w''(\ell) \rrbracket = \llbracket w'''(\ell) \rrbracket = 0, \quad (6)$$

where $\llbracket f(\ell) \rrbracket$ denotes $f(\ell^+) - f(\ell^-)$.

The final required condition should concern the energy required to advance the delamination, which, together with the adhesive resistive of the beam–substrate interface, can determine the delamination length ℓ . We then follow Griffith's concept for linear fracture mechanics [54] and calculate the energy release rate G of the system by examining the instantaneous loss of total potential energy Π per unit delamination growth. As detailed in Appendix A, we find:

$$G = \frac{1}{2} k_W u^2 \Big|_{x=\ell}. \quad (7)$$

Note that the energy release rate in the case of rigid substrate has been reported as:

$$G_{\text{Rigid}} = \frac{1}{2} B w''^2 \Big|_{x=\ell}, \quad (8)$$

according to [3,25]. Therefore, the presence of a deformation substrate improves the smoothness of the beam's deflection from the class of C^1 to C^3 . In this work, we limit ourselves by overlooking the mode-mixity [38] and the interfacial imperfections [55–58] and considering a constant critical energy release or adhesion energy γ . It is obvious that real interfaces often exhibit various imperfections, such as surface roughness, interfacial slip, and internal debonding, we acknowledge that these factors can influence adhesion behavior. The impacts of such imperfections should be addressed in conjunction with experimental results for a more accurate assessment. In this study, we focus on the effects of substrate elasticity and long-range interfacial forces on adhesion. By assuming perfect adhesion, we can simplify our analysis and direct our attention toward understanding how these specific factors influence the adhesion mechanics. Therefore, the last boundary condition to complete the problem is then

$$G = \gamma. \quad (9)$$

2.2. Dugdale-type approach

For structures at small scales, the long-range interfacial interactions are expected to play a role [30,38,59]. Following the concept of Dugdale or cohesive model in fracture mechanics, we replace the discrete beam–substrate interaction in Eq. (2) with retarded London–van der Waals forces, taking the form of Lennard-Jones potentials [60]:

$$p = \frac{9}{2} \frac{\gamma}{s_0} \left[\left(\frac{s_0}{w - w_s} \right)^4 - \left(\frac{s_0}{w - w_s} \right)^{10} \right], \quad (10)$$

where s_0 is the equilibrium spacing at the atomic scale. It is noted that different potentials, such as the non-retarded Lennard-Jones, Buckingham potentials, and registry-depended potentials may provide a more accurate description of the complex interfacial interactions. However, we stick to Eq. (10) in this work which would allow for some analytical progress. With Eq. (10), separating the beam from the substrate from equilibrium spacing to infinity requires an energy γ per unit area. In this Dugdale-type approach, there is no clear delamination or adhesion front, as illustrated in Fig. 2b; therefore, we define the delamination length via the position where the substrate shows the largest surface deformation (labeled by the pink solid marker in Fig. 2b). Besides, the surface deformation of the substrate no longer equals the deflection of the beam—they are through the distributed load p given in Eq. (10):

$$p = k_W(w_s + s_0). \quad (11)$$

Apparently, as the substrate becomes rigid (i.e., $k_W \rightarrow \infty$), w_s approaches $-s_0$ in the defined coordinate system.

2.3. The transition to the steady state

The Griffith-type and Dugdale-type models presented here account for the spring-like deformation of the substrate, resulting in qualitatively different boundary conditions compared to curvature jump conditions observed with rigid substrates. However, for a prescribed end deflection δ , we anticipate a significant delamination length ℓ . It should be noted that the prescribed end deflection δ has been set small enough to ensure that the stored elastic energy in the delamination process is always dominated by bending energy [61,62]. This setting makes the problem we considered here much like the bending-dominated blister test (such as in [63]) rather than the stretching-dominated peeling test (such as in [14,15]). In such case, the elastic energy stored in the substrate remains unchanged upon advancing the delamination front, leading to a steady state where the substrate elasticity no longer plays a role in determining the energy release rate. Essentially, under the same critical energy release rate γ , the results of both Griffith-type and Dugdale-type model for deformable substrate should gradually converge towards the results of rigid substrates as δ or ℓ increases. Hence, a key question to be answered is by which parameter this transition takes place.

We will demonstrate that this transition parameter can be defined by comparing characteristic horizontal lengths within the delamination region and the contact region. The relevant horizontal length scale in the delamination region $0 < x < \ell$ is relatively straightforward since it is ℓ itself. A way to relate this length to more intrinsic properties of the system is to compare the elastic energy stored in the beam $\sim B\delta^2/\ell^4 \times \ell$ with the adhesion energy $\sim \gamma \times \ell$. This comparison leads to a bendoadhesive or elastocapillary length [3]:

$$\ell_{ec} = (B\delta^2/\gamma)^{1/4}. \quad (12)$$

In fact, previous work on the same configuration, illustrated in Fig. 2a, but with rigid substrates, has shown [18,20]:

$$\ell_{Rigid} = 18^{1/4} \ell_{ec}. \quad (13)$$

The next task is to uncover the deformation characteristics of the beam in the contact region, taking into account the effects of substrate elasticity and long-range interfacial forces, which will be the focus of the remainder of this paper.

3. Griffith-type model: Effect of the substrate elasticity

3.1. A Winkler length scales

We first address the length scales in the system with deformable substrates. There are two key horizontal length scales to consider: one in the delamination region (i.e., the elastocapillary length ℓ_{ec} already given in Eq. (12)) and the other in the contact region. For $x > \ell$, Eqs. (1) and (2) indeed suggest a Winkler length,

$$\ell_W = (B/k_W)^{1/4}. \quad (14)$$

over which the beam deflects the elastic substrate. It is natural to compare the two horizontal length scales in the two regions:

$$K_W = \left(\frac{\ell_{ec}}{\ell_W} \right)^4 = \frac{k_W \delta^2}{\gamma}. \quad (15)$$

This parameter can be thought of as the effective stiffness of the substrate, which is interestingly independent of the bending stiffness of the beam. We then expect that for small γ or large k_W or δ , $K_W \gg 1$ and the calculated ℓ should approach ℓ_{Rigid} given in Eq. (13).

3.2. Non-dimensionalization

The primary interest is the delamination length under prescribed δ . We then use δ and elastocapillary length ℓ_{ec} to rescale the system. Specifically, we perform the following:

$$X = x/\ell_{ec}, \quad W = w/\delta, \quad P = p\delta/\gamma, \quad L = \ell/\ell_{ec}. \quad (16)$$

We then obtain the dimensionless form of the problem

$$W'''' + K_W W H(X - L) = 0, \quad (17)$$

for $0 \leq X < \infty$, subject to

$$\begin{aligned} W(0) &= 1, & W'(0) &= 0, & W(X \rightarrow \infty) &= W'(X \rightarrow \infty) = 0, \\ \|W(L)\| &= \|W'(L)\| = \|W''(L)\| = \|W'''(L)\| = 0, \end{aligned} \quad (18)$$

and a critical condition to solve for the delamination length

$$\frac{1}{2} K_W W^2(L) = 1. \quad (19)$$

Eqs. (17) to (19) complete the problem, which relies exclusively on the effective substrate stiffness K_W defined in Eq. (15).

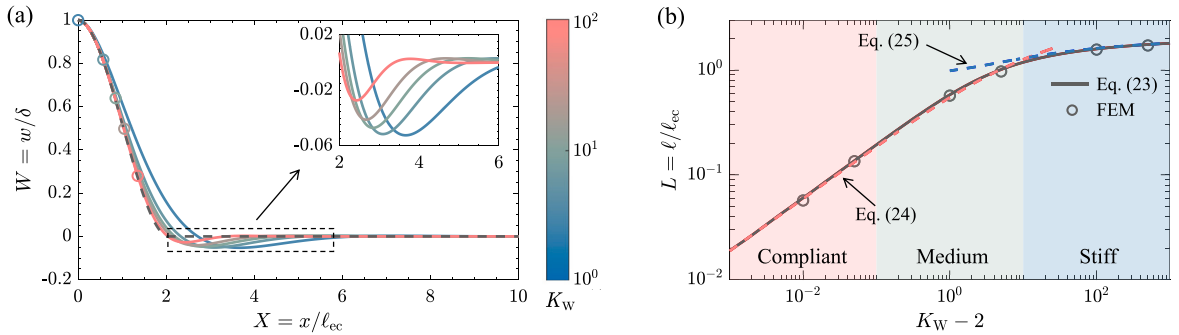


Fig. 3. Griffith-type modeling of the adhesion of the beam on a thin elastic substrate. (a) The dimensionless deflection of the beam for various effective substrate stiffness K_W . The solid curves represent the analytical given by Eqs. (20)–(22). The colored markers indicate the detachment fronts. The black dashed curve denotes the result for a rigid substrate. (b) The dimensionless detachment length as a function of the effective substrate stiffness. The solid curve is plotted using the analytical solution given in Eq. (23). The dashed curves are based on asymptotic results of the solution as $K_W \rightarrow 2$ (given in Eq. (24)) and $K_W \rightarrow \infty$ (given in Eq. (25)). The markers represent results obtained using the finite element calculation discussed in Section 3.4.

3.3. Analytical solutions

The analytical solution to Eqs. (17) to (19) can be readily obtained with the boundary conditions in Eq. (18):

$$W(X) = (a_1 X^3 + a_2 X^2 + 1) \mathcal{H}(L - X) + e^{\xi(L-X)} (b_1 \sin \xi X + b_2 \cos \xi X) \mathcal{H}(X - L), \quad (20)$$

where $\xi = (K_W/4)^{1/4}$, and a_i and b_i ($i = 1, 2$) are integration constants. We apply the matching conditions in Eq. (18) to obtain

$$a_1 = \frac{2\xi^3}{3 + L\xi [3 + L\xi(3 + L\xi)]}, \quad a_2 = -\frac{3\xi^2(1 + L\xi)}{3 + L\xi [3 + L\xi(3 + L\xi)]}, \quad (21)$$

and

$$b_1 = \frac{(1 - L\xi) \cos L\xi + (1 + L\xi) \sin L\xi}{1 + L\xi [1 + L\xi(1 + L\xi/3)]}, \quad b_2 = \frac{(1 + L\xi) \cos L\xi - (1 - L\xi) \sin L\xi}{1 + L\xi [1 + L\xi(1 + L\xi/3)]}. \quad (22)$$

Finally, using the condition Eq. (19), we obtain an expression for the delamination length:

$$L = (4/K_W)^{1/4} [G(K_W) - 1] + K_W^{1/4}/G(K_W), \quad (23)$$

where

$$G(K_W) = \left(\sqrt{1 - \sqrt{2}K_W^{3/2}/4} - 1 \right)^{1/3}.$$

The calculated deflection of the beam with different substrate stiffness K_W are plotted in Fig. 3a (denoted by colored solid curves). Also included are the corresponding delamination fronts (denoted by colored markers). As expected, the calculated results converge to the rigid substrate limit denoted by the dashed curve as $K_W \gg 1$. Alternatively, we find a discernible substrate deformation near the delamination front (see enlarged view in Fig. 3a). Such substrate deformation leads to a reduced delamination length of the system (see the colored markers). Interestingly, we find that the delamination occurs or the problem has a solution only when $K_W \geq 2$; otherwise the adhesion-caused substrate deformation can completely fill the gap prescribed by the end displacement δ .

We further plot the analytical $L - K_W$ relation given in Eq. (23) in Fig. 3b (denoted by solid curve). To gain a more explicit understanding of the K_W dependency of the delamination length, we seek an asymptotic solution to Eq. (23) by setting $K_W = 2 + \tilde{K}_W$ with $|\tilde{K}_W| \ll 1$. This gives

$$L = 2^{-3/4} (K_W - 2)^{1/2} \quad \text{as} \quad K_W \rightarrow 2, \quad (24)$$

which is also presented in Fig. 3b (the red dashed curve). Notably, Eq. (24) agrees with the full solution quite well even at $K_W \sim 10$. However, as the effective substrate stiffness becomes very large, we need to seek the solution to Eq. (23) with $1/K_W \ll 1$. This leads to

$$L = 18^{1/4} - (4/K_W)^{1/4} \quad \text{as} \quad K_W \gg 1, \quad (25)$$

which is plotted as the blue dashed curve in Fig. 3b. Note that $18^{1/4}$ is solution for rigid substrates (see Eq. (13)). These findings demonstrate that K_W can be used as a transition parameter to connect the results for elastic and rigid substrates.

3.4. Comparison with finite element analysis

We note the simple analytical solutions above are based on by assuming a spring-like response for the elastic substrate. The validity of this assumption requires a large slenderness of the substrate, i.e., $d \ll \ell_W$ for the problem we consider [51], or

$$S = \frac{(1-2\nu)B}{(1-\nu)Gd^3} \gg 1, \quad (26)$$

in dimensional form. Therefore, though the controlling parameter K_W in our problem is independent of the mechanical properties of the beam, the bending stiffness of the beam is important in the accuracy of our analytical solutions. In addition, since the Winkler stiffness in Eq. (3) is obtained based on linear elasticity theory, we require $|w| \ll d$ in the entire domain. Considering the maximum deflection occurs at the delamination front, this requirement, according to Eqs. (7) and (9), can be satisfied by

$$\mathcal{L} = \frac{(1-2\nu)\gamma}{(1-\nu)Gd} \ll 1. \quad (27)$$

To further justify the results of the Griffith-type model, we employ a cohesive zone model to simulate this interface delamination problem with finite element method (FEM) (see Fig. B.7). Following the experiments reported in [32], we adopt the properties of the glass for the beam and polymeric films for the thin elastic substrate that is perfectly bonded to its bottom surface. A typical bilinear cohesive law is used with $\gamma = 40 \text{ mJ/m}^2$ (see more details in Appendix B) [64]. The substrate with shear modulus $G = 1 \text{ MPa}$, thickness $d = 100 \mu\text{m}$, and the beam with flexural rigidity $B = 5 \times 10^{-3} \text{ N m}$ are used in our computation. In this context, $S \sim 10^3$ and $\mathcal{L} \sim 10^{-3}$, satisfying the requirements by Eqs. (26) and (27) simultaneously. We use different gap heights to tune the effective stiffness of the substrate ($K_W = 2.01, 2.05, 3, 7, 102$ and 502). Excellent agreement is found between the FEM results (denoted by the markers) and the Griffith-type model in Fig. 3b.

4. Effect of the long-range forces

4.1. Van der Waals length scales

For 2D material-based semiconductor devices illustrated in Fig. 1c, it is more appropriate to adopt the Dugdale-type approach discussed in Section 2.2 to understand the adhesion behavior of the beam. By introducing a Lennard-Jones type vdW potential in Eq. (10), we eliminate the need to assume macroscopic delaminated and contact regions. Furthermore, long-range interfacial traction introduces new length scales that warrant further discussion.

Firstly, similar to the Winkler foundation model for thin elastic substrates, the interfacial traction in Eq. (10) can be considered as an array of independent, nonlinear springs. The linearization of such potential for $|w - w_s| \ll s_0$ can also give a stiffness for the vdW springs:

$$k_{\text{vdW}} = \frac{\gamma}{s_0^2}, \quad (28)$$

Along the line to reach the Winkler length ℓ_W in Eq. (14), we obtain a horizontal, vdW length:

$$\ell_{\text{vdW}} = \left(\frac{B}{k_{\text{vdW}}} \right)^{1/4} = \left(\frac{Bs_0^2}{\gamma} \right)^{1/4}. \quad (29)$$

In addition, the vdW potential involves an intrinsic vertical length, namely the equilibrium spacing s_0 . Interestingly, when comparing the vertical lengths in the “delaminated” region and the vdW region, we find

$$\mu = \left(\frac{\ell_{\text{ec}}}{\ell_{\text{vdW}}} \right)^2 = \frac{\delta}{s_0}, \quad (30)$$

which is conceptually identical to comparing the horizontal lengths in the “delaminated” region and the vdW region.

We may perceive μ as a transition parameter that characterizes whether the adhesion behavior of the systems is macroscopic ($\mu \gg 1$) or microscopic ($\mu \ll 1$). However, μ alone is not exclusive, as the effect of the substrate elasticity has not been considered yet. This can be illustrate by normalizing the vdW potential following Eq. (16):

$$P = \frac{9\mu}{2} \left[\frac{1}{\mu^4 (W - W_s)^4} - \frac{1}{\mu^{10} (W - W_s)^{10}} \right], \quad (31)$$

where the substrate deformation $W_s \neq W$ in this Dugdale-type model is also part of the solution to be determined with the additional Winkler equation (11), which has the dimensionless form:

$$P = K_W(W_s + 1/\mu). \quad (32)$$

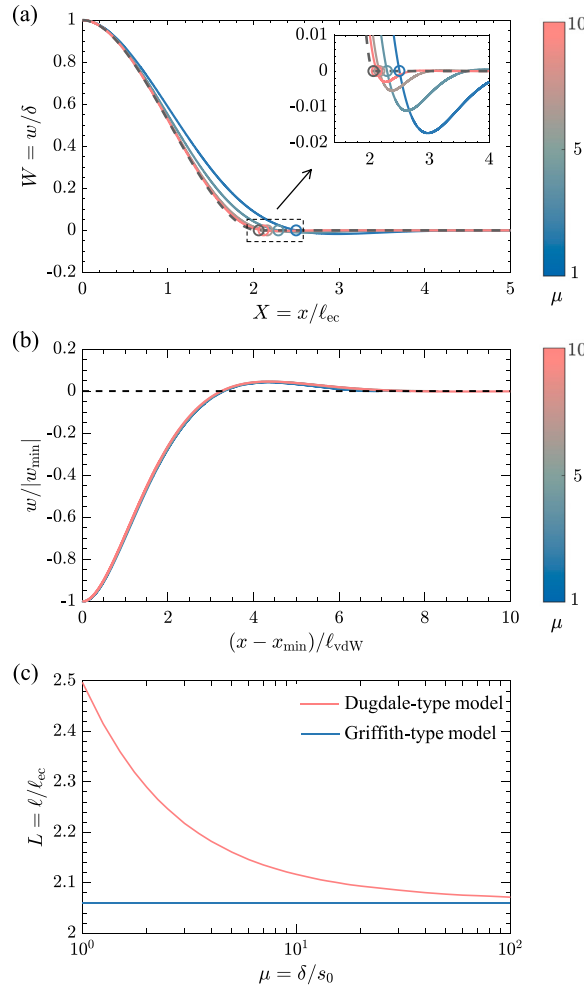


Fig. 4. Stiction of the plate with a rigid foundation at small scale described by the Dugdale-type model. (a) The solid curves are obtained by numerically solving Eq. (34) subjected to Eq. (35) for various μ . The colored markers indicate the detachment points for various μ . The dashed line denotes the result of the JKR-type model with a rigid substrate; (b) The solid curves represent the deflection of the plate for various μ at the defined contact region, where the y axis is rescaled by the absolute value of w_{\min} and the x axis is rescaled by the relative to x_{\min} by ℓ_{vdW} ; (c) Evolution curve of detachment length L for various μ obtained from the Dugdale-type model with a rigid substrate, accompanied by the result of the JKR-type model.

4.2. The rigid substrate

We first focus on a limiting case where the substrate deformation is negligible so that $w_s \equiv -s_0$ or $W_s \equiv -1/\mu$ (Fig. 2b). According to Eqs. (31) and (32), this requires $K_W \gg \mu^2$, i.e.,

$$k_W \gg k_{\text{vdW}} \quad \text{or} \quad k_W s_0^2 \gg \gamma \quad (33)$$

in a physical sense. The problem is then largely simplified as

$$W'''' + \frac{9\mu}{2} \left[\frac{1}{(\mu W + 1)^4} - \frac{1}{(\mu W + 1)^{10}} \right] = 0, \quad (34)$$

subject to

$$W(0) = 1, \quad W'(0) = 0, \quad W(\infty) = 0, \quad W'(\infty) = 0. \quad (35)$$

In this simplified problem, μ does become the only transition parameter.

In Fig. 4a, we plot the calculated deflections of the beam for various μ . It is evident that as μ increases, the deflection curves approach the dashed curve calculated based on the Griffith-type model for rigid substrates, which involves solving the beam equation with the jump condition described in Eq. (8). Additionally, similar to the adhesion behavior on an elastic substrate, the beam exhibits a slight concave downward deflection due to the deformation of the vdW springs as the delaminated beam approaches the

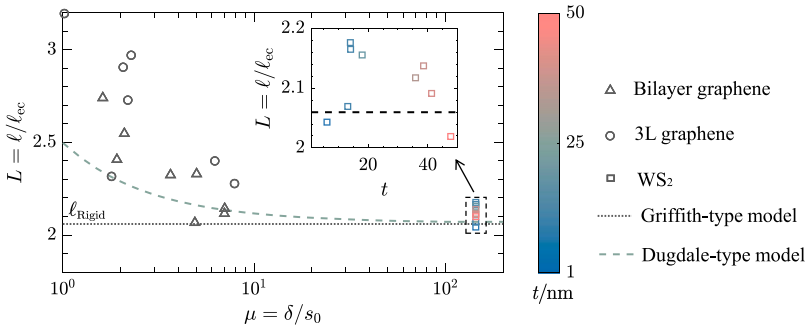


Fig. 5. Experimental results on the detachment behavior of two-dimensional layered materials adhered to substrates with varying gap heights. The horizontal axis represents the gap height, while the vertical axis shows the dimensionless detachment length. Circular markers correspond to experimental results for bilayer graphene, and triangular markers represent three-layer (3L) graphene, both from Ref. [65]. Square markers indicate results for WS_2 with different thicknesses adhered to a SiO_2 substrate, as reported in Ref. [8].

equilibrium spacing (see zoom-in view in Fig. 4a). The appropriate length scale to observe this concave shape is not ℓ_{ec} but rather ℓ_{vdW} instead. This can also be confirmed by linearizing the governing Eq. (34) as

$$W'''' + 27\mu^2 W = 0, \quad (36)$$

suggesting that $X \sim \mu^{-1/2}$ or $x \sim \ell_{\text{vdW}}$ in the “contact” region. We define the location of the smallest downward deflection as x_{\min} and the corresponding deflection as w_{\min} . In Fig. 4b, we re-plot the concave shape by rescaling the y axis by the absolute value of w_{\min} and rescaling the x axis relative to x_{\min} by ℓ_{vdW} , resulting in a master curve that confirms the deflection of the van der Waals springs occurs over ℓ_{vdW} .

Unlike the decreased delamination length induced by Winkler springs as shown in Fig. 3b, nonlinear vdW springs appear to increase the apparent delamination length as seen in Fig. 4a. To quantify this, we define the delamination front in the Dugdale model with rigid substrates as the point where the beam–substrate gap first reaches the equilibrium spacing s_0 , when subjected to the prescribed δ at $x = 0$. The delamination fronts are indicated by colored markers in Fig. 4a and summarized in Fig. 4c as a function of μ . From a microscopic perspective on adhesion, a process zone of size ℓ_{vdW} is required for the interface to be considered delaminated in this Dugdale-type model. When the size of this process zone is negligible compared to the characteristic length scale ℓ_{ec} , i.e.,

$$\mu \gg 1$$

according to Eq. (30), the long-range effect of vdW force can be neglected. Consequently, the delamination length reverts to the Griffith-type result for a rigid substrate ℓ_{Rigid} , as given in Eq. (13) and represented by the red line in Fig. 4c.

To further validate the transition from Dugdale-type to Griffith-type behavior from an experimental perspective, and to capture the influence of long-range vdW forces, we have analyzed the experimental results from Refs. [8] and [65]. The relationship between the dimensionless detachment length and the dimensionless height is presented in Fig. 5. The circular markers represent bilayer graphene, and the triangular markers represent three-layer (3L) graphene from the experimental results in Ref. [65]. It is evident that the height has a significant effect on the detachment length due to the strong long-range van der Waals forces at small gap heights $\mu \sim 1$. The deviation between experimental results and our Dugdale-type model might be due to the unusual bending stiffness of few-layer graphene and the complex interfacial interactions that cannot be captured by simple LJ-type potential [38]. Additionally, experimental results for tungsten disulfide (WS_2) with various thicknesses adhered to a silicon oxide substrate (SiO_2) with a gap height of 48 nm have been analyzed [8]. It can be concluded that the dimensionless detachment lengths for various thicknesses are close to the analytical result of the Griffith-type model i.e., ℓ_{Rigid} . As the gap height increases, the effect of the long-range vdW forces weakens, leading to a transition from a Dugdale-type model to a Griffith-type model.

4.3. The deformable substrate

Finally, we consider microbeam adhesion by accounting for both substrate elasticity and long-range interfacial forces. Building on the understanding developed in the previous subsections, we now discuss the characteristic horizontal length in the “contact” region. The connection of Winkler springs with vdW springs suggests an effective spring stiffness of

$$k_{\text{eff}} = \frac{27k_W k_{\text{vdW}}}{k_W + 27k_{\text{vdW}}}. \quad (37)$$

We added a prefactor of 27 here, according to the linearized vdW spring equation (36), to have a more precise description of the vdW spring constant. As a result, the corresponding characteristic length can be obtained as

$$\ell_{\text{eff}} = \left(\frac{B}{k_{\text{eff}}} \right)^{1/4} = \left[\frac{B (k_W s_0^2 + 27\gamma)}{27k_W \gamma} \right]^{1/4}. \quad (38)$$

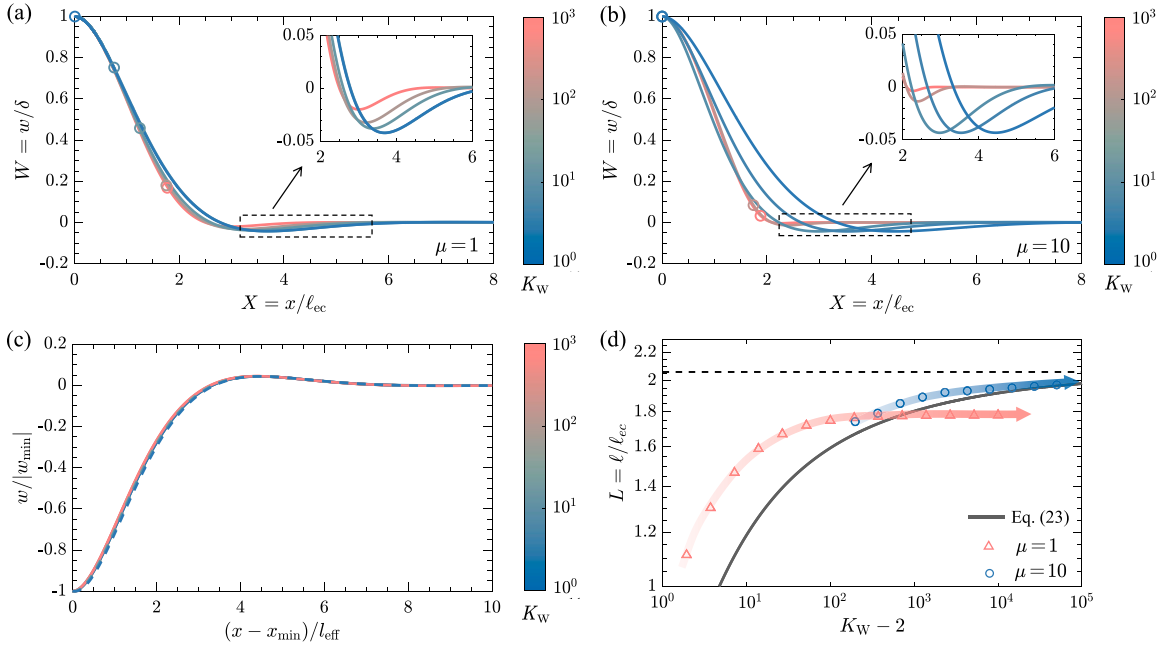


Fig. 6. Stiction of the plate with a deformable substrate at small scale described by the Dugdale-type model. (a) The solid curves are obtained by numerically solving Eq. (40) for various K_W using $\mu = 1$. The colored markers indicate the detachment points; (b) $\mu = 10$; (c) The curves represent the deflection of the plate for various K_W at the defined contact region, where the y axis is rescaled by the absolute value of w_{\min} and the x axis is rescaled by x_{\min} by ℓ_{eff} , the solid lines are the results obtained by using $\mu = 1$ and the dashed lines are using $\mu = 10$; (d) Comparison of the detachment length L of the JKR-type model (solid curve) and the Dugdale-type model (colored markers) for various K_W using $\mu = 1$ and 10, respectively.

Clearly, $\ell_{\text{eff}} \rightarrow 3^{-3/4} \ell_{\text{vdW}}$ if Eq. (33) is satisfied and $\ell_{\text{eff}} \rightarrow \ell_W$ vice versa. Comparing the elastocapillary length ℓ_{ec} with this effective length in the contact region, we have

$$\mu_{\text{eff}} = \left(\frac{\ell_{\text{ec}}}{\ell_{\text{eff}}} \right)^4 = \frac{27k_W\delta^2}{k_W s_0^2 + 27\gamma} = \frac{27K_W\mu^2}{K_W + 27\mu^2}, \quad (39)$$

which should be the combined transition parameter for the Dugdale-type model of elastic substrates. It is also conceptually similar to K_W for Griffith-type model of elastic substrates in Eq. (15) when $k_W \ll k_{\text{vdW}}$ (or $K_W \ll \mu^2$) and to μ for Dugdale-type model of rigid substrates in Eq. (30) when $k_W \gg k_{\text{vdW}}$ (or $K_W \gg \mu^2$).

According to Eqs. (1), (10), (11), and the nondimensionalization (16), the problem in this Dugdale-type model of elastic substrates is to solve

$$W'''' + K_W(W_s + 1/\mu) = 0, \\ \frac{2K_W}{9\mu^2}(\mu W_s + 1) - \frac{1}{\mu^4 (W - W_s)^4} + \frac{1}{\mu^{10} (W - W_s)^{10}} = 0, \quad (40)$$

subject to boundary conditions in Eq. (35), which depends on both μ and K_W . We then plot numerically calculated deflections of the beam for various K_W using $\mu = 1$ in Fig. 6a and using $\mu = 10$ in Fig. 6b. Again, we observe a concave downward deflection of the beam in the contact region and define the location of the smallest downward deflection as w_{\min} and the corresponding deflection as x_{\min} . Rescaling this downward deflection by $w/|w_{\min}|$ and $(x - x_{\min})/\ell_{\text{eff}}$ give rise to a master curve for all calculated data (Fig. 6c), suggesting that the effective length ℓ_{eff} perfectly characterizes the horizontal length scale in this problem.

The delamination front $X = L$ is defined by the position where the substrate shows the maximum surface deformation, as illustrated in Fig. 2b. We present the delamination lengths for a range of K_W and two particular values of μ (1 and 10) in Fig. 6d. Based on the previous discussion, we may treat μ as a transition parameter between microscopic and macroscopic adhesion behavior, K_W as a transition parameter between elastic and rigid substrates, and μ_{eff} as a combined transition parameter toward the rigid substrate with macroscopic adhesion behavior. This can be further confirmed by the results (denoted by markers) for the Dugdale-type model with elastic substrates in Fig. 6d: A large μ is required for them to approach the Griffith-type model with elastic substrates (the solid curve given by Eq. (23)), while both large μ and K_W are needed to ensure a large μ_{eff} , allowing them to approach the Griffith-type model with rigid substrates $\ell = (18)^{1/4} \ell_{\text{ec}}$ given in Eq. (13) [18,20]. For example, in the case of a commonly used elastic substrate like PDMS (with a shear modulus of ~ 1 MPa and a thickness of 1 μm), the transition from Dugdale-type to Griffith-type adhesion occurs when the gap height reaches approximately 1 μm . Similarly, for two-dimensional layered materials (with an elastic modulus of ~ 30 GPa and a thickness of 1 nm), the transition occurs when the gap height reaches around 1 nm.

5. Conclusion

In this study, we explored the adhesion behavior of microbeams on elastic substrates, focusing on the impact of substrate elasticity and long-range interfacial forces. We developed and analyzed Griffith-type and Dugdale-type models to understand the critical adhesion conditions and behavior. We found that all these models could converge to the well-studied classical stiction problem with a rigid substrate via a defined transition parameter. This parameter encompasses two length scales: the characteristic bendoadhesive or elastocapillary length in the delaminated region, and either the Winkler length, van der Waals length, or a combined length, depending on the specific effects of substrate elasticity and long-range interfacial forces. We found that substrate deformation could decrease the delamination length, while the use of long-range interfacial forces increased the apparent delamination length. Although our results focused on a simple configuration illustrated in Fig. 2, we expect that the theoretical framework developed to address the impact of substrate elasticity and long-range interfacial forces can readily extend to various other configurations in engineering systems such as micro/nano-electromechanical systems, micro/nano-fluidics, and wearable electronics involving soft adhesive layers or very small length scales.

The relatively simple framework of our Griffith-type and Dugdale-type models has facilitated the exploration of a few critical aspects of the delamination of beams from elastic substrates. However, our analysis does not account for a number of failure mechanisms that can occur during delamination in practice. For example, complex three-dimensional failure modes, such as fingering instabilities, internal debonding, and unstable crack propagation [66,67], may arise during the delamination process. Additionally, the adhesive layer such as polymers and the microbeam such as graphite can exhibit plastic, poroelastic, and viscoelastic behaviors near the crack tip, which can significantly affect the delamination criterion [68,69]. These factors cannot be captured by the simple models used in this work.

CRediT authorship contribution statement

Hang Li: Writing – original draft, Methodology, Investigation, Formal analysis. **Zhaohe Dai:** Writing – review & editing, Methodology, Investigation, Formal analysis, Conceptualization.

Declaration of competing interest

The authors declare that they have no known competing financial interests or personal relationships that could have appeared to influence the work reported in this paper.

Acknowledgments

This work was financially supported by the National Natural Science Foundation of China (Grant No. 12372103, 12302076, and 12432003).

Appendix A. Energy release rate

Based on the Griffith's concept for linear fracture mechanics, for the beam on an elastic substrate under displacement-controlled conditions (i.e., prescribed end displacement illustrated in Fig. 2a), we can write the total potential energy of the system as

$$\Pi = U_f + U_s, \quad (\text{A.1})$$

where

$$U_f = \int_0^\infty \frac{1}{2} B w''^2 dx$$

is the bending energy stored in the beam, and

$$U_s = \int_\ell^\infty \frac{1}{2} k_W w_s^2 dx$$

is the elastic energy stored in the substrate. To calculate the energy release rate, we apply the variational principle to the total energy Π with movable ℓ : $\delta\Pi = \delta U_f + \delta U_s$. Integration by parts leads to

$$\begin{aligned} \delta U_f &= \int_0^\ell B w''' \delta w dx + \int_\ell^\infty B w''' \delta w dx + \\ &B \delta w' w''|_0^\ell - B \delta w w'''|_0^\ell + B \delta w' w''|_\ell^\infty - B \delta w w'''|_\ell^\infty + \frac{1}{2} B w'' \Big|_{\ell^-} \delta \ell - \frac{1}{2} B w'' \Big|_{\ell^+} \delta \ell, \end{aligned} \quad (\text{A.2})$$

and

$$\delta U_s = \int_\ell^\infty k_W w_s \delta w_s dx - \frac{1}{2} k_W w_s^2|_{\ell^+} \delta \ell. \quad (\text{A.3})$$

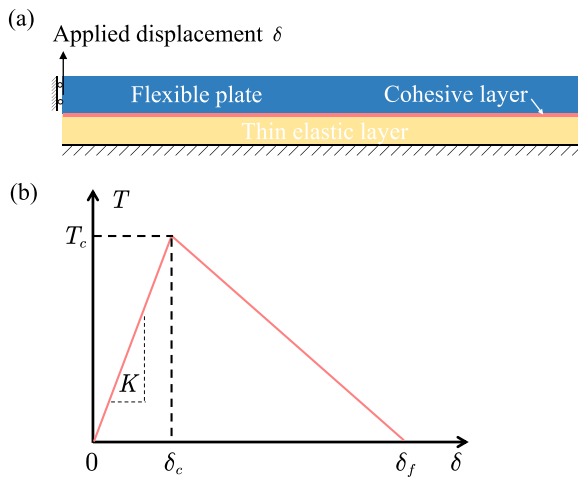


Fig. B.7. (a) Schematic illustration of the model in finite element simulations; (b) A bilinear traction–separation law is used to characterize the delamination of the interface.

By setting $\delta w \neq 0$ for $x < \ell$ and $\delta w = \delta w_s \neq 0$ for $x > \ell$, we arrive at the equilibrium Eqs. (1) and (2). According to the chain rule, we have $\delta w|_\ell = \delta w(\ell) - w'(\ell)\delta\ell$ and $\delta w'|_\ell = \delta w'(\ell) - w''(\ell)\delta\ell$. Together with natural matching conditions given in Eq. (6), we find that

$$\delta\Pi = -\frac{1}{2}k_W w^2 \Big|_{x=\ell} \delta\ell. \quad (\text{A.4})$$

The energy release rate can be immediately calculated by

$$\mathcal{G} = -\frac{\delta\Pi}{\delta\ell}, \quad (\text{A.5})$$

giving Eq. (7) in the main text. It should be noted that following the JKR-type approach, we can write the total free energy as

$$\mathcal{F} = U_f + U_s + \gamma\ell. \quad (\text{A.6})$$

We can also obtain the adhesion condition given in Eqs. (7) and (9) by minimizing the total free energy.

Appendix B. Finite element analysis

The simulation can be performed in commercial finite element software (such as ABAQUS). The geometry of the beam and the substrate is constructed with $10 \times 0.2 \times 0.13 \text{ mm}^3$ and $10 \times 0.2 \times 0.1 \text{ mm}^3$, respectively. The beam and substrates are isotropic elastic materials, where their shear moduli are set 10^4 MPa and 1 MPa , respectively. The cohesive elements are used to initially bond the beam and the substrate together. A typical bilinear cohesive law is used in the finite element simulation with normal peak traction $T_c = 0.1 \text{ MPa}$, the slope $K = 10^4 \text{ MPa/mm}$. The interface fracture energy is set as $\gamma = 40 \text{ mJ/m}^2$ according to Ref. [33]. The maximum nominal stress criterion is adopted to describe the initiation of the damage and the energy-based evolution is used to describe the damage process. Different gap heights at left end of the beam are used in order to achieve various detachment lengths. It is important to mention that the critical fracture energies in the shear directions have been set to a sufficient level to ensure the fracture behavior is dominated by the normal deformation (see Fig. B.7).

Data availability

Data will be made available on request.

References

- [1] Israelachvili JN. Intermolecular and surface forces. 3rd ed. 2011.
- [2] Freund LB, Suresh S. Thin film materials: stress, defect formation and surface evolution. Cambridge University Press; 2004.
- [3] Bico J, Reyssat É, Roman B. Elastocapillarity: When surface tension deforms elastic solids. *Annu Rev Fluid Mech* 2018;50:629–59.
- [4] Style RW, Jagota A, Hui C-Y, Dufresne ER. Elastocapillarity: Surface tension and the mechanics of soft solids. *Annu Rev Condens Matter Phys* 2017;8:99–118.
- [5] Dai Z, Liu L, Zhang Z. Strain engineering of 2D materials: Issues and opportunities at the interface. *Adv Mater* 2019;31(45):1805417.
- [6] Chortos A, Liu J, Bao Z. Pursuing prosthetic electronic skin. *Nature Mater* 2016;15(9):937–50.
- [7] Geim AK. Exploring two-dimensional empty space. *Nano Lett* 2021;21(15):6356–8.

- [8] Ronceray N, Spina M, Chou VHY, Lim CT, Geim AK, Garaj S. Elastocapillarity-driven 2D nano-switches enable zeptoliter-scale liquid encapsulation. *Nature Commun* 2024;15(1):185.
- [9] Kang M-C, Rim C-S, Pak Y-T, Kim W-M. A simple analysis to improve linearity of touch mode capacitive pressure sensor by modifying shape of fixed electrode. *Sensors Actuators A* 2017;263:300–4.
- [10] Fragiacomo G, Ansbaek T, Pedersen T, Hansen O, Thomsen EV. Analysis of small deflection touch mode behavior in capacitive pressure sensors. *Sensors Actuators A* 2010;161(1–2):114–9.
- [11] Li Y, Zhu M, Bandari VK, Karnaushenko DD, Karnaushenko D, Zhu F, et al. On-chip batteries for dust-sized computers. *Adv Energy Mater* 2022;12(13):2103641.
- [12] Schmidt CK, Medina-Sánchez M, Edmondson RJ, Schmidt OG. Engineering microrobots for targeted cancer therapies from a medical perspective. *Nature Commun* 2020;11(1):5618.
- [13] Obreimoff J. The splitting strength of mica. *Proc R Soc A* 1930;127(805):290–7.
- [14] Peng Z, Wang C, Chen L, Chen S. Peeling behavior of a viscoelastic thin-film on a rigid substrate. *Int J Solids Struct* 2014;51(25–26):4596–603.
- [15] Peng Z, Yin H, Yao Y, Chen S. Effect of thin-film length on the peeling behavior of film-substrate interfaces. *Phys Rev E* 2019;100(3):032804.
- [16] Gong Y, Li S, Liu J. Peeling of an extensible soft microbeam to solid: large deformation analysis. *Int J Appl Mech* 2018;10(06):1850065.
- [17] Mastrangelo C, Hsu C. Mechanical stability and adhesion of microstructures under capillary forces-Part I: Basic Theory. *J Microelectromech Syst* 1993;2(1):33–43.
- [18] Mastrangelo C, Hsu C. Mechanical stability and adhesion of microstructures under capillary forces-Part II: Experiments. *J Microelectromech Syst* 1993;2(1):44–55.
- [19] Mastrangelo C. Adhesion-related failure mechanisms in micromechanical devices. *Tribol Lett* 1997;3(3):223–38.
- [20] De Boer M, Michalske T. Accurate method for determining adhesion of cantilever beams. *J Appl Phys* 1999;86(2):817–27.
- [21] Jones EE, Begley MR, Murphy KD. Adhesion of micro-cantilevers subjected to mechanical point loading: Modeling and experiments. *J Mech Phys Solids* 2003;51(8):1601–22.
- [22] Rogers JW, Mackin TJ, Phinney LM. A thermomechanical model for adhesion reduction of MEMS cantilevers. *J Microelectromech Syst* 2002;11(5):512–20.
- [23] Fang W, Mok J, Kesari H. Effects of geometric nonlinearity in an adhered microbeam for measuring the work of adhesion. *Proc R Soc A* 2018;474(2211):20170594.
- [24] Li H, Yu C, Dai Z. Regimes in the axisymmetric stiction of thin elastic plates. *Int J Mech Sci* 2024;284:109740.
- [25] Glassmaker N, Hui C. Elastica solution for a nanotube formed by self-adhesion of a folded thin film. *J Appl Phys* 2004;96(6):3429–34.
- [26] Majidi C. Remarks on formulating an adhesion problem using Euler's elastica (draft). *Mech Res Commun* 2007;34(1):85–90.
- [27] Majidi C, Adams GG. A simplified formulation of adhesion problems with elastic plates. *Proc R Soc A* 2009;465(2107):2217–30.
- [28] Okegbu DO, Kardomateas GA. Large deflection effects on the energy release rate and mode partitioning of the single cantilever beam sandwich debond configuration. *J Appl Mech* 2024;91(1):011001.
- [29] Nguyen MH, Kardomateas GA. Elastic foundation solution for the end-notched flexure mode II sandwich configuration. *J Appl Mech* 2024;91(11):111006.
- [30] Liu Z, Liu JZ, Cheng Y, Li Z, Wang L, Zheng Q. Interlayer binding energy of graphite: A mesoscopic determination from deformation. *Phys Rev B* 2012;85(20):205418.
- [31] Wagner TJ, Vella D. Switch on, switch off: Stiction in nanoelectromechanical switches. *Nanotechnology* 2013;24(27):275501.
- [32] Ghatak A, Mahadevan L, Chaudhury MK. Measuring the work of adhesion between a soft confined film and a flexible plate. *Langmuir* 2005;21(4):1277–81.
- [33] Skotheim J, Mahadevan L. Soft lubrication. *Phys Rev Lett* 2004;92(24):245509.
- [34] Sun Y, Chen R, Wang W, Zhang J, Qiu W, Liu X, et al. Rate-dependent pattern evolution in peeling adhesive tape driven by cohesive failure. *Langmuir* 2022;38(42):12785–94.
- [35] Li D, Chen M, Zong Q, Zhang Z. Floating-gate manipulated graphene-black phosphorus heterojunction for nonvolatile ambipolar Schottky junction memories, memory inverter circuits, and logic rectifiers. *Nano Lett* 2017;17(10):6353–9.
- [36] Liu L, Kong L, Li Q, He C, Ren L, Tao Q, et al. Transferred van der Waals metal electrodes for sub-1-nm MoS₂ vertical transistors. *Nat Electron* 2021;4(5):342–7.
- [37] Juel A, Pihler-Puzović D, Heil M. Instabilities in blistering. *Annu Rev Fluid Mech* 2018;50(1):691–714.
- [38] Dai Z, Lu N, Liechti KM, Huang R. Mechanics at the interfaces of 2D materials: Challenges and opportunities. *Curr Opin Solid State Mater Sci* 2020;24(4):100837.
- [39] Wu E, Xie Y, Liu Q, Hu X, Liu J, Zhang D, et al. Photoinduced doping to enable tunable and high-performance anti-ambipolar MoTe₂/MoS₂ heterotransistors. *ACS Nano* 2019;13(5):5430–8.
- [40] Mishchenko A, Tu J, Cao Y, Gorbachev RV, Wallbank J, Greenaway M, et al. Twist-controlled resonant tunnelling in graphene/boron nitride/graphene heterostructures. *Nature Nanotechnology* 2014;9(10):808–13.
- [41] Zhang Y, Zhao Y. A precise model for the shape of an adhered microcantilever. *Sensors Actuators A* 2011;171(2):381–90.
- [42] Zhang Y, Zhao Y. Flexural contact in MEMS stiction. *Int J Solids Struct* 2012;49(17):2203–14.
- [43] Long H, Liu Y, Wei Y. Debonding characterization of stiff film/compliant substrate systems based on the bilinear cohesive zone model. *Eng Fract Mech* 2022;265:108363.
- [44] Perrin H, Eddi A, Karpitschka S, Snoeijer JH, Andreotti B. Peeling an elastic film from a soft viscoelastic adhesive: Experiments and scaling laws. *Soft Matter* 2019;15(4):770–8.
- [45] Mukherjee B, Batra RC, Dillard DA. Edge debonding in peeling of a thin flexible plate from an elastomer layer: A cohesive zone model analysis. *J Appl Mech* 2017;84(2):021003.
- [46] Ciceri G. A general approach for modelling the peeling of a flexible tape from an elastic substrate. *Int J Solids Struct* 2023;273:112277.
- [47] Li B, Cao Y, Feng X, Gao H. Mechanics of morphological instabilities and surface wrinkling in soft materials: a review. *Soft Matter* 2012;8(21):5728–45.
- [48] Yu C, Dai Z. Premature jump-to-contact with elastic surfaces. *J Mech Phys Solids* 2024;193:105919.
- [49] Dillard DA. Bending of plates on thin elastomeric foundations. *J Appl Mech* 1989;56(2):382–6.
- [50] Ghatak A, Chaudhury MK. Adhesion-induced instability patterns in thin confined elastic film. *Langmuir* 2003;19(7):2621–31.
- [51] Chandler TG, Vella D. Validity of Winkler's mattress model for thin elastomeric layers: Beyond Poisson's ratio. *Proc R Soc A* 2020;476(2242):20200551.
- [52] Li J, Zhang G, Dai Z. Indentation of a plate on a thin transversely isotropic elastic layer. *Acta Mech Solida Sin* 2024;1–10.
- [53] Argatov I, Mishuris G, Argatov I, Mishuris G. Deformation of a thin bonded transversely isotropic elastic layer. In: Contact mechanics of articular cartilage layers: Asymptotic models. Springer; 2015, p. 1–18.
- [54] Griffith AA. VI. The phenomena of rupture and flow in solids. *Philos Trans R Soc Lond A Contain Pap Math Phys Character* 1921;221(582–593):163–98.
- [55] Ghatak A, Mahadevan L, Chung JY, Chaudhury MK, Shenoy V. Peeling from a biomimetically patterned thin elastic film. *Proc R Soc Lond Ser A Math Phys Eng Sci* 2004;460(2049):2725–35.
- [56] Athanasiou CE, Zhang H, Ramirez C, Xi J, Baba T, Wang X, et al. High toughness carbon-nanotube-reinforced ceramics via ion-beam engineering of interfaces. *Carbon* 2020;163:169–77.
- [57] Gao W, Huang R. Effect of surface roughness on adhesion of graphene membranes. *J Phys D: Appl Phys* 2011;44(45):452001.
- [58] Kardomateas G, Pelegri A, Malik B. Growth of internal delaminations under cyclic compression in composite plates. *J Mech Phys Solids* 1995;43(6):847–68.

- [59] Yuan X, Zhao P, Fan Q. The peeling behavior of compliant nano-films in adhesive contact with a planar rigid substrate: Insights from molecular dynamics and continuum mechanics. *Thin-Walled Struct* 2024;112272.
- [60] Casimir HB, Polder D. The influence of retardation on the London-van der Waals forces. *Phys Rev* 1948;73(4):360.
- [61] Chen E, Dai Z. Axisymmetric peeling of thin elastic films: A perturbation solution. *J Appl Mech* 2023;90(10):101011.
- [62] Dai Z. Analytical solutions for circular elastic membranes under pressure. *J Appl Mech* 2024;91(8):081002.
- [63] Wan K-T. Fracture mechanics of a shaft-loaded blister test-transition from a bending plate to a stretching membrane. *J Adhes* 1999;70(3–4):209–19.
- [64] Yin H, Liang L, Wei Y, Peng Z, Chen S. Determination of the interface properties in an elastic film/substrate system. *Int J Solids Struct* 2020;191:473–85.
- [65] Han E, Yu J, Annevelink E, Son J, Kang DA, Watanabe K, et al. Ultrasoft slip-mediated bending in few-layer graphene. *Nat Mater* 2020;19(3):305–9.
- [66] Juel A, Pihler-Puzović D, Heil M. Instabilities in blistering. *Annu Rev Fluid Mech* 2018;50(1):691–714.
- [67] Athanasiou CE, Liu X, Zhang B, Cai T, Ramirez C, Padture NP, et al. Integrated simulation, machine learning, and experimental approach to characterizing fracture instability in indentation pillar-splitting of materials. *J Mech Phys Solids* 2023;170:105092.
- [68] Freund LB, Suresh S. Thin film materials: stress, defect formation and surface evolution. Cambridge University Press; 2004.
- [69] Dong W, Dai Z, Liu L, Zhang Z. Toward clean 2d materials and devices: Recent progress in transfer and cleaning methods. *Adv Mater* 2024;36(22):2303014.